UC Irvine
UC Irvine Previously Published Works

Title

The role of feedback in the formation of morphogen territories

Permalink

https://escholarship.org/uc/item/5p4139wp

Journal

Mathematical Biosciences and Engineering, 5(2)

ISSN

1547-1063

Authors

Iron, David

Syed, Adeela

Theisen, Heidi

et al.

Publication Date

2008

DOI

10.3934/mbe.2008.5.277

Copyright Information

Peer reviewed

The Role of Feedback in the Formation of Morphogen Territories

David Iron[a], **Adeela Syed**[b], **Heidi Theisen**[b], **Tamas Lukacsovich**[b], **Mehrangiz Naghibi**[a], **Lawrence J. Marsh**[b], **Fred Wan**[c], and **Qing Nie**[c]

[1]Dalhousie University, Department of Mathematics and Statistics

[2]University of California, Irvine, Department of Developmental and Cell Biology

[3]University of California, Irvine, Center for Mathematical and Computational Biology and Department of Mathematics

Abstract

In this paper, we consider a mathematical model for the formation of spatial morphogen territories of two key morphogens: Wingless (Wg) and Decapentaplegic (DPP), involved in leg development of Drosophila. We define a gene regulatory network (GRN) that utilizes auto-activation and cross inhibition (modeled by Hill equations) to establish and maintain stable boundaries of gene expression. By computational analysis we find that in the presence of a general activator, neither auto-activation, nor cross inhibition alone are sufficient to maintain stable sharp boundaries of morphogen production in the leg disc. The minimal requirements for a self-organizing system are a coupled system of two morphogens in-which the auto-activation and cross-inhibition have Hill coefficients strictly greater than one. In addition, the GRN modeled here describes the regenerative responses to genetic manipulations of positional identity in the leg disc.

Keywords

Pattern formation; Gene regulatory network; Dynamical systems; Partial differential equations

1 Introduction

A key biological question of current interest is how cells within a field acquire spatial information. The acquisition of this positional identity is important for normal development and growth. It is also key to understanding regeneration. The signals which specify positional information are secreted proteins called morphogens. Abnormal signaling by these proteins can lead to developmental abnormalities and cancer.

Reaction diffusion systems have been used to model stages of embryonic development since the seminal works of Gierer and Meinhardt [4,5]. In these papers it is shown that long range inhibition coupled with short range activation can lead to complex patterns of morphogen distribution which in turn will lead to formation of localized structures. Recently, details of the biochemical reactions which occur in developmental biology have been discovered, including estimates of many of the key parameters. In this paper, we will examine the mechanisms discussed in [6], namely cross-inhibition and auto-activation of the production rates of the morphogens Wingless and Decapentaplegic. The modeling of these mechanisms will be based as closely as possible on the known biochemical reactions and using the best available parameter estimates.

Correspondence to: David Iron.

The Drosophila leg imaginal disc can be used to illustrate pattern formation, which is the acquisition of positional information by cells. Drosophila has six leg imaginal discs that become patterned during the larval stage and then undergo morphogenesis in the pupal stage to form the six legs of the y. Each leg imaginal disc is a single layered field of cells that integrate positional information from three morphogens, WNT/WINGLESS (WG), DECAPENTAPLEGIC (DPP)/BMP, and HEDGEHOG (HH). Dorsal/Ventral (D/V) positional information is specified by antagonizing inputs from the dorsally expressed morphogen, DPP, and the ventrally expressed morphogen, WG[22,1,9,10,19,20,23,6]. The distal tip of the leg, where the dorsal and ventral territories abut each other is specified by the integration of Wg and Dpp signaling. Abnormal expression of these genes causes patterning defects in flies and developmental defects and cancer in humans.

Since restricted expression of these morphogens is critical for normal patterning, the domain of production of these proteins must be maintained as the disc grows. Here we model the GRN that maintains the mutually exclusive DPP/BMP and WG expression domains during development and reestablishes these territories in response to injury or genetic manipulations. The secreted signals that form this GRN are HH which is expressed in the posterior compartment, WG which is expressed in a ventral wedge in the anterior compartment and DPP/BMP which is expressed in a dorsal stripe in the anterior compartment (Fig 1). Activation of *wg* and *dpp* gene expression, i.e. the production of WG and DPP/BMP, requires HH signaling. WG signaling inhibits ventral production of DPP[22,23,21,6,1,10], and DPP signaling inhibits dorsal production of WG[1,9,20,23], thus setting up a dorsal DPP expressing territory and a ventral WG expressing territory. WG and DPP have also been shown to autoactivate their own production [2,6,30,1,8,19,11,24]. We have generated a computational model for this GRN and used it to test the requirements for auto-activation and cross inhibition in maintaining stable domains of expression.

In this model, the domains of production of WG and DPP have sharp boundaries. The free morphogen can diffuse away from this domain and form a gradient of morphogen signaling. The domain of Wg production (Wp) is a function of WG signaling (WR) and DPP/BMP signaling (BR), where WR represents WG bound to its receptor and BR represents DPP/BMP bound to its receptor. Similarly, the domain of DPP/BMP expression (Bp) is a function of WR and BR. In this system, DPP/BMP acts as a dimer, which results in similar diffusivity coefficients for WG and DPP. This differs from a Turing-Meinhardt model, which predicts that the diffusion constants for two interacting morphogens are different, often by several orders of magnitude [25,17,12]. The objective of the modeling is to determine the elements of a GRN required to establish stable sharp mutually exclusive boundaries of expression of two morphogens from an initial shallow gradient of morphogen concentration. The initial shallow gradient is formed by processes discussed in [14,15]. Once this shallow gradient is formed, the combination of auto-activation and cross-inhibition will cause the gradients to steepen until two distinct territories are formed.
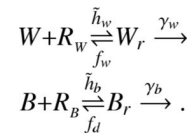
We now compare and contrast some of the recent mathematical models of GRNs in Drosophila. In [13], it is shown that a single diffusible morphogen with localized production and interaction with its receptor can lead stable spatial gradients of morphogen concentration. In [16,18] it is shown that the presence of a competing ligand can increase the strength of the spatial morphogen concentration gradient. In [15], a well defined production region is shown to result in the formation of shallow spatial gradients. In [26] positive feedback acting through a cell-surface bound BMP-binding protein can result in sharp gradients. In this paper, we will consider two morphogens interacting with their respective receptors. Morphogen production rate will be regulated by only auto-activation and cross-inhibition, and both the feedbacks are assumed to be functions of bound morphogen. In the system, there are no spatially dependent parameters.

1.1 A model and equations

The Drosophila leg initially develops as a flattened disc with dorsal DPP/BMP and ventral WG production domains, which respectively define dorsal and ventral territories. The disc is also divided into an anterior and posterior compartment defined by the absence or presence respectively of engrailed expression. The center of the disc will form the distal tip of the leg and the outer edge will form the proximal leg structures. At this stage the disc can be treated as a 2D structure. In Figure 1, we show the geometry of a leg imaginal disc, and the domains of gene expression/protein production of wg and dpp/bmp. To simplify the analysis, we consider a one-dimensional system in the dorsal-ventral direction as illustrated in (Figure 1 (b)).

In this system, the following assumptions are made: (a) DPP/BMP and WG are produced in the entire domain. (b) Both WG and DPP/BMP diffuse freely from the site of production. (c) BMP/DPP and WG associate with their respective receptors, RB (Tkv/Punt/Sax) and RW (Fz) to form receptor-ligand complexes with defined association and dissociation rates. (d) The receptors and the receptor-ligand complexes do not diffuse (e) The receptor-ligand complexes are degraded at the same rate throughout the field. (f) Receptor bound Wg (Wr) and receptor bound DPP/BMP (Br) respectively stimulate the production (gene expression) of WG (Wp) and DPP/BMP (Bp) (g) WG and BMP/DPP respectively inhibit the production (gene expression) of WG (Wp) and BMP/DPP (Bp)

The bio-chemical reactions for receptor ligand interaction are as follows,

$$W + R_w \underset{f_w}{\overset{\tilde{h}_w}{\rightleftharpoons}} W_r \overset{\gamma_w}{\longrightarrow}$$

$$B + R_B \underset{f_d}{\overset{\tilde{h}_b}{\rightleftharpoons}} B_r \overset{\gamma_b}{\longrightarrow} \, .$$

Applying the law of mass action, the number of receptors available to bind with ligand is RW - Wr and RB - Br for WG and BMP respectively. We will model the unbound morphogens as freely diffusing chemicals and the bound morphogens as spatially fixed. Thus the dynamics of the model are given by the following system of differential equations.

$$W_t = D_w W_{xx} - \tilde{h}_w (R_W - W_r) W + f_w W_r + \text{Act}(W_r) \, \text{Inh}(B_r), \tag{1a}$$

$$W_{\mathrm{rt}} = \tilde{h}_w (R_W - W_r) W - (f_w + \gamma_w) W_r, \tag{1b}$$

$$B_t = D_b B_{xx} - \tilde{h}_b (R_B - B_r) B + f_b B_r + \text{Act}(B_r) \, \text{Inh}(W_r), \tag{1c}$$

$$B_{\mathrm{rt}} = \tilde{h}_b (R_B - B_r) B - (f_b + \gamma_b) B_r, \tag{1d}$$

$$-x_{\max} < x < x_{\max}, t > 0, \tag{1e}$$

$$\frac{\partial W}{\partial x}=\frac{\partial B}{\partial x}=0, \text{ at } x= \pm x_{\max}.$$

(1f)

We have assumed no-flux boundary conditions for WG and DPP, because far from the interface, the concentration of the morphogens is roughly constant. The activation function (Act) smoothly connects a minimum production value to a maximum and is strictly increasing, while the inhibition function (Inh) connects a maximum production value to a minimum production value and is strictly decreasing. These functions will be further defined later (Section 3). Representing the feedback as the product of the activation and inhibition function implies that the auto-activation and cross-inhibition mechanisms are linked.

1.2 Scaling

In sections §4.1 we will use asymptotic methods to construct a solution and analyze its stability. In order to perform this analysis, we will need to know the relative orders of each of the terms in (1). We will now scale the variables to normalize the solution and the length of the domain. We thus set,

$$y=\frac{x}{x_{\max}},$$

(2)

$$w=(y,t)=\frac{W(yx_{\max},t)}{R_W},$$

(3)

$$b(y,t)=\frac{B(yx_{\max},t)}{R_B},$$

(4)

$$w_r(y,t)=\frac{W_r(yx_{\max},t)}{R_W},$$

(5)

$$b_r(y,t)=\frac{B_r(yx_{\max},t)}{R_B}.$$

(6)

We now define the new paremeters as,

$$\overline{D}_W=\frac{D_W}{(x_{\max})^2} \quad \overline{D}_B=\frac{D_B}{(x_{\max})^2}$$
$$h_w=\frac{\tilde{h}_w}{R_W} \quad h_B=\frac{\tilde{h}_B}{R_B}$$

Since the diffusivities $\overline{D_D}$ and $\overline{D_W}$ are small and equal, we will let $\epsilon^2 = \overline{D_D} = \overline{D_W}$ and use ϵ as an asymptotically small parameter. With this choice, we expect the thickness of the transition layer to be $O(\epsilon)$. The new equations may new be written as,

$$w_t = \epsilon^2 w_{yy} - h_w(1 - w_r)w + f_w w_r + \text{Act}(w_r)\, \text{Inh}(b_r),$$

(7a)

$$w_{rt} = h_w(1 - w_r)w - (f_w + \gamma_w)w_r,$$

(7b)

$$b_t = \epsilon^2 b_{yy} - h_b(1 - b_r)b + f_b b_r + \text{Act}(b_r)\, \text{Inh}(w_r),$$

(7c)

$$b_{rt} = h_b(1 - b_r)b - (f_b + \gamma_b)b_r,$$

(7d)

$$-1 < y < 1\,, t > 0\,,$$

(7e)

$$\frac{\partial w}{\partial y} = \frac{\partial b}{\partial y} = 0,\ \text{at } y = \pm 1.$$

(7f)

The remainder of the paper will proceed as follows. In §2 we will consider spatially homogeneous equilibrium solutions of (7). In §3, we consider explicit forms of the feedback functions. In §4, we will consider a simplification which reduces the model to two uncoupled second order differential equations. We will show that it is possible to construct a territoried solution with a single morphogen, but such a solution will not be sufficiently robust. We will also show that even if such a solution exists, it will be unstable. In §5 we will give some numerical results and compare with experimental results. Finally, we will discuss the relevance of the results for the simplified system to the full coupled systems and consider further avenues of study.

2 Construction of Solution

We are interested in steady state solutions with two distinct regions. In one of the regions, corresponding to the dorsal region, b will be a relatively large constant and w a smaller constant value. In the other region, corresponding to the ventral region, w will be the large constant and b will have a smaller constant value. These regions will be connected by a thin layer in which both w and b concentrations will have steep gradients. As a first step in the construction of a solution, we look at the spatially constant steady-states.

Before we can proceed, we must first provide some details for the functions Act and Inh. We let,

$$K_{\max} = \lim_{u \to 0+} \text{Inh}(u) = \lim_{u \to \infty} \text{Act}(u),$$
$$K_{\min} = \lim_{u \to 0+} \text{Act}(u) = \lim_{u \to \infty} \text{Inh}(u).$$

In the most general case, each instance of Act(u) and Inh(u) may have distinct limits, but as this generalization will only make the notation more cumber-some, we will not consider it here.

We now find the values of the steady state solution in the two regions (dorsal and ventral). In the dorsal region, the value of b_r will be relatively high and w_r relatively low. Thus, in this region, the terms $\mathrm{Act}(w_r)\,\mathrm{Inh}(b_r) \approx K_{\min}^2$ and $\mathrm{Act}(b_r)\,\mathrm{Inh}(w_r) \approx K_{\max}^2$. In these regions, the solution is constant, so the diffusion terms will all be zero. The steady state equations in the dorsal region are then,

$$0 = -h_w(1-w_r)w + f_w w_r + K_{\min}^2, \tag{8}$$

$$0 = h_w(1-w_r)w - (f_w+\gamma_w)w_r, \tag{9}$$

$$0 = -h_b(1-b_r)b + f_b b_r + K_{\max}^2, \tag{10}$$

$$0 = h_b(1-b_r)b - (f_b+\gamma_b)b_r. \tag{11}$$

The solution to the above system is given by,

$$\overline{w} = \frac{(f_w+\gamma_w)K_{\min}^2}{h_w(\gamma_w - K_{\min}^2)}, \tag{12a}$$

$$\overline{w}_r = \frac{K_{\min}^2}{\gamma_w}, \tag{12b}$$

$$\overline{b} = \frac{(f_b+\gamma_b)K_{\max}^2}{h_b(\gamma_b - K_{\max}^2)}, \tag{12c}$$

$$\overline{b}_r = \frac{K_{\max}^2}{\gamma_b}. \tag{12d}$$

We may repeat the process in the ventral region to find the ventral steady state values:

$$\widehat{w} = \frac{(f_w+\gamma_w)K_{\max}^2}{h_w(\gamma_w - K_{\max}^2)}, \tag{13a}$$

$$\widehat{w}_r = \frac{K_{\max}^2}{\gamma_w}, \tag{13b}$$

$$\widehat{b} = \frac{(f_b + \gamma_b)K^2_{\min}}{h_b(\gamma_b - K^2_{\min})},$$

(13c)

$$\widehat{b}_r = \frac{K^2_{\min}}{\gamma_b}.$$

(13d)

Note, we will require $\gamma_b > K^2_{\min/\max}$ and $\gamma_w > K^2_{\min/\max}$ for a positive solution.

For a steady state solution connecting these two equilibria to exist, each equilibrium must itself be stable in the absence of diffusion. Thus, we set ϵ to zero and linearize about (12) and (13). The eigenvalues of this linearization are given by,

$$\lambda_1 = \frac{-a \pm \sqrt{a^2 - 4h_w(\gamma_w - K^2_{\max})}}{2}, \quad a = h_w\left(1 - \frac{K^2_{\max}}{\gamma_w} + \frac{f_w + \gamma_w}{h_W}\left(\frac{\gamma_w}{\gamma_w - K^2_{\max}}\right)\right) > 0,$$

$$\lambda_2 = \frac{-a \pm \sqrt{a^2 - 4h_b(\gamma_b - K^2_{\min})}}{2}, \quad a = h_b\left(1 - \frac{K^2_{\min}}{\gamma_b} + \frac{f_b + \gamma_b}{h_B}\left(\frac{\gamma_b}{\gamma_b - K^2_{\min}}\right)\right) > 0,$$

$$\lambda_3 = \frac{-a \pm \sqrt{a^2 - 4h_w(\gamma_w - K^2_{\min})}}{2}, \quad a = h_w\left(1 - \frac{K^2_{\min}}{\gamma_w} + \frac{f_w + \gamma_w}{h_w}\left(\frac{\gamma_w}{\gamma_w - K^2_{\text{mmin}}}\right)\right) > 0,$$

$$\lambda_4 = \frac{-a \pm \sqrt{a^2 - 4h_b(\gamma_b - K^2_{\max})}}{2}, \quad a = h_w\left(1 - \frac{K^2_{\max}}{\gamma_b} + \frac{f_B + \gamma_b}{h_B}\left(\frac{\gamma_b}{\gamma_b - K^2_{\max}}\right)\right) > 0.$$

For the equilibria to be stable we need the real parts of the above eigenvalues to be negative. The two restrictions $\gamma_b > K^2_{\min/\max}$ and $\gamma_w > K^2_{\min/\max}$ imply that all the steady states must be stable.

3 Feedback

We now consider an explicit form for the functions Act and Inh. We require that the activation function goes from K_{min} to K_{max} monotonically and the inhibition function goes from K_{max} to K_{min} monotonically, where $K_{max} > K_{min} > 0$. We will characterize these functions with four parameters. The two parameters K_{min} and K_{max}, have already been discussed. The two remaining parameters will control the sharpness of the transition (from K_{max} to K_{min}) and the point at which the transition occurs.

The most critical parameter value is the point at which the activation and inhibition switches off/on. If this value is too high or low, the activation/inhibition will have no effect. We can find an appropriate value by considering the values of b_r and w_r. Since $0 \le w_r, b_r \le 1$, we may set the switching value to $\frac{1}{2}$.

A natural choice for the activation and inhibition functions are,

$$\text{Act}(u) = \frac{K_{\max} - K_{\min}}{1 + \left(\frac{u}{u_0}\right)^{-m}} + K_{\min},$$

(14)

$$\text{Inh}(u) = \frac{K_{\max} - K_{\min}}{1 + \left(\frac{u}{u_0}\right)^m} + K_{\min}.$$

(15)

Here m controls the steepness of the transition and is referred to as the Hill coefficient. u_0 controls the value at which the transition occurs, for our application, we set $u_0 = \frac{1}{2}$. This form of activation/inhibition was first considered by Archibald Hill in [7]. The basis for this form of activation/inhibition is considering the simultaneous binding of m ligands to an enzyme to produce a product which will either initiate or inhibit protein production. The fact that simultaneous binding is required makes choices of m large unreasonable [29]. Using a negative Hill coefficient for inhibition is considered in [28].

We will now consider the conditions necessary for the formation of morphogen territories with this feed-back model. A morphogen territoried solution corresponds to a heteroclinic connection between two equilibria of the system. To find the conditions which will allow for such a connection, we consider a simplification. When we consider steady-state solutions, (7) reduces to two second order differential equations which are coupled by the inhibition functions. To simplify the system, we take the inhibition function to be a constant and thus decouple the equations.

4 Heteroclinic Connection: The simplified system

In this section, we will construct a heteroclinic connection for a system in which the Inh function is a constant. This will reduce the steady state problem for (7) to a single second order ordinary differential equation. We find levels of inhibition which will result in a heteroclinic connection between two states. The existence of a heteroclinic orbit in the situation of a constant inhibition field will require a specific isolated value of inhibition, and thus the heteroclinic will not be robust. Further, we show that any such connection will be unstable.

To simplify our situation, we will consider the case $\text{Inh}(x) = I$ where I is some constant. We now look for steady state solutions with a heteroclinic connection. Since w_r does not diffuse, we may solve for w_r in terms of w and eliminate it from the equation.

$$w_r(w) = \frac{w}{\beta + w},$$

(16)

where $\beta = \frac{\gamma_w + f_w}{h_w}$. We plug into the steady-state equation for w to get,

$$\epsilon^2 w_{yy} + Q(w; I) = 0,$$

(17)

where,

$$Q(w; I) = \frac{-2^m \gamma_w w_r(w)^{m+1} + 2^m I\, K_{\max} w_r(w)^m - \gamma_w w_r - \gamma_w w_r + I\, K_{\min}}{2^m w_r(w)^m + 1}.$$

(18)

I will leave $w_r(w)$ as a function in the equations to simplify the analysis. We note that the function $w_r(w) : \mathbb{R}^+ \to [0, 1)$ is one-to-one and onto.

We now consider some general results for the existence of heteroclinic connections. For an equation of the form,

$$u'' + Q(u) = 0, \tag{19}$$

to have a heteroclinic connection (a front solution) joining the values $u = u_-$ to $u = u_+$, the following restrictions on $Q(u)$ must be met:

1. $Q(u)$ must have 3 consecutive roots u_-, u_0, and u_+ with $u_- < u_0 < u_+$.

2. $Q'(u_-) < 0$, $Q'(u_+) < 0$ and $Q'(u_0) > 0$.

3. $\int_{u_-}^{u_+} Q(u)du = 0$

The constructed heteroclinic orbit will connect the two states $u = u_-$ and $u = u_+$ as $y \to \pm\infty$.

The system we are considering is posed on a finite domain, and is of the form so the $\epsilon^2 w_{yy} + Q(w; I) = 0$. First we apply the coordinate change $z = \frac{y}{\epsilon}$ to magnify the region about the interface.

The equation then will be of the form $w_{zz} + Q(w) = 0$ with $w_z(\pm\frac{1}{\epsilon}) = 0$. If we assume that we can satisfy the conditions necessary for the existence of a heteroclinic orbit, the constructed orbit will fail to satisfy the boundary conditions, but only by exponentially small terms. We may thus expect a solution to exist which is exponentially close to the constructed heteroclinic. In §4.1 we will carefully consider the effects of the finite boundary on the stability of the constructed solution.

Now we will examine the polynomial in the numerator of $Q(w; I)$,

$$P(w_r) = -2^m \gamma_w w_r^{m+1} + 2^m I K_{\max} w_r^m - \gamma_w w_r + I K_{\min}, \tag{20}$$

to determine the conditions which will ensure the existence of a heteroclinic orbit. For $Q(w; I)$ to have 3 positive roots, (20)(as a function of w_r) must have 3 roots in $(0, 1)$. This immediately implies that $m \geq 2$. This result agrees with numerical observations (see Figure 5). We will assume now $m \geq 2$. Descartes' rule of signs implies that (20) has exactly one or three positive real roots (counting multiplicity). If m is even, we have no negative roots and if m is odd we will have exactly one negative root.

If we assume that we have 3 distinct roots in $(0, 1)$, the second constraint will be satisfied due to the sign of the highest power of w_r and the fact that the denominator of Q is positive and increasing. We will label the three roots w_{r-}, w_{r0} and w_{r+} where $w_{r-} < w_{r0} < w_{r+}$. We denote the corresponding values of w as, w_-, w_0 and w_+.

We find necessary and sufficient condition for (20) to have 3 distinct roots in $(0, 1)$. We will not give this condition in an explicit form as the resulting expression is cumbersome and provides no illumination. We let w_{rmax} be the value at which P attains its local maximum.

$$w_{\text{rmax}}(I) = \frac{2I K_{\max} + \sqrt{4I^2 K_{\max}^2 - 3\gamma^2}}{6\gamma}. \tag{21}$$

We now let $\bar{I}$ be the value of I for which $P(w_{rmax}(\bar{I})) = 0$. So for all three roots to be in $(0, 1)$, we require that $w_{rmax}(\bar{I}) < 1$. If this condition is met then for $I > \bar{I}$ and $I - \bar{I}$ sufficiently small, all three roots of $P(w_r)$ must lie in $(0, 1)$.

We must satisfy one final condition to ensure the existence of the heteroclinic orbit. We need to satisfy the integral condition $\int_{w_-}^{w_+} Q(w;I)\mathrm{dw}=0$. We would like to have a large range of I values for which all three roots will be in $(0, 1)$ as this will make it easier to solve the integral condition. The closer w_{rmax} is to $\frac{1}{2}$ at $I = \bar{I}$, the easier it will be to satisfy the integral condition (this will result in a larger interval of I values for which we will have three positive roots in $(0, 1)$. Finding an explicit restriction on parameter values which are necessary and sufficient for the satisfaction of this condition does not seem possible. The difficulty lies in the fact that changing the value of I to satisfy the integral condition may cause w_{r+} to move past 1.

We demonstrate that it is quite simple to find a value of I which satisfies the integral condition and for which the three roots of (20) are in $(0, 1)$. We will use the same rate and diffusion constants before but with $m = 2$, but we can pick K_{max} and K_{min}. To check the integral condition, we make the change of variables $w=\dfrac{\beta w_r}{1 - w_r}$. Then the integral condition is,

$$\int_{w_{r-}}^{w_{r+}} \frac{\beta P(w_r)}{(4w_r{}^2+1)(1 - w_r)^2}\mathrm{dw}_r=0. \tag{22}$$

Using numerical integration is sufficient to determine if there are values of I for which the above integral is negative and values for which it is positive. We set $K_{min} = 0.001$ and $K_{max} = 0.051$ [1] . Using $I = 0.01$, we have the following zeros of $P(w_r)$,

$$w_{r-} \approx 0.0219, w_{r0} \approx 0.3544, w_{r+} \approx 0.6437. \tag{23}$$

and

$$\int_{w_{r-}}^{w_{r+}} \frac{\beta P(w_r)}{(4w_r{}^2+1)(1 - w_r)^2}\mathrm{dw}_r \approx 0.0000063 \tag{24}$$

For $I = 0.0097$ we get the three zeros of $P(w_r)$ to be,

$$w_{r-} \approx 0.0211, w_{r0} \approx 0.4145, w_{r+} \approx 0.5537. \tag{25}$$

and

$$\int_{w_{r-}}^{w_{r+}} \frac{\beta P(w_r)}{(4w_r{}^2+1)(1 - w_r)^2}\mathrm{dw}_r \approx -0.00007056 \tag{26}$$

---

[1]Although it appears that $\gamma_w < K_{min}^2$ and thus there shouldn't even be two positive homogeneous solutions, this is not really the case here. The value we need to consider in the inequalities are not $K_{max/min}^2$, but $K_{max/min}I$

Hence there must be a value of *I* for which the integral condition is satisfied exactly and maintains the root condition. We can solve for the heteroclinic orbit implicitly. We can write (17) as a first order system,

$$w\prime = u, \tag{27}$$

$$u\prime = -Q(w). \tag{28}$$

This system is Hamiltonian with Hamiltonian function $H(w, u) = \frac{1}{2}u^2 + \int_{w_-}^{w} Q(s;I)\,\mathrm{d}s$. With this choice of Hamiltonian function, the heteroclinic orbit is given by $H(w, u) = 0$. Thus,

$$u^2 = (w\prime)^2 = -2\int_{w_0}^{w} Q(s;I)\,\mathrm{d}s. \tag{29}$$

We can solve this equation implicitly to find the following implicit expression for the heteroclinic orbit:

$$\int_{w_-}^{w} \frac{d\omega}{\pm\sqrt{-2\int_{w_0}^{\omega} Q(s;I)\,\mathrm{d}s}} = y \tag{30}$$

The $\pm$ determines which heteroclinic we find with the plus sign corresponding to a connection from w_- to w_+. We can solve this integral numerically to get the profile for the heteroclinic orbit (see Figure 3).

The existence of this solution requires a specific value of *I*. This implies that the front will be structurally unstable. Any small change in inhibition will mean that the connecting steady-state solution will cease to exist.

4.1 Stability of Heteroclinic

We now examine the stability of the heteroclinic orbit constructed in the previous section. We constructed the heteroclinic orbit on an unbounded domain. However, it will fail to satisfy the boundary conditions on any finite domain by exponentially small terms. We can expect a solution to exist on a bounded domain that is exponentially close to the constructed heteroclinic. To study the stability of this orbit, we will construct an eigenvalue problem by linearizing about the constructed solution. We will show the operator associated with the linearization will have an exponentially small eigenvalue. This eigenvalue is related to the translation invariance of the interface when the problem is posed on an unbounded domain. We estimate the eigenvalue in the limit $\epsilon \to 0$ and show it is positive, but exponentially small. So although the orbit is unstable, it can persist for an extremely long time.

First we list some asymptotic estimates for the behaviour of the heteroclinic solution. We assume we have a heteroclinic connection given by $w_H\left(\frac{y}{\epsilon}\right)$. Then we have that,

$$w_H\left(\frac{y}{\epsilon}\right) \sim w_\pm \mp a_\pm e^{\mp \epsilon^{-1}\nu_+ y} \text{ as } y \to \pm\infty, \tag{31}$$

where

$$\nu_{\pm} = \sqrt{-Q\prime(w_{\pm})} \tag{32}$$

$$\log(a_{\pm}) = \log(|w_0 - w_{\pm}|) \pm \int_{w_0}^{w_{\pm}} \left(\frac{\nu_{\pm}}{\sqrt{2\int_{w_-}^z -Q(\zeta)d\zeta}} + \frac{1}{z - w_{\pm}} \right) dz \tag{33}$$

Now we construct the associated eigenvalue problem by linearizing about the heteroclinic orbit.

$$w = w_H + \phi(y)e^{\lambda t}, \tag{34}$$

and substitute (34) into (17) to get the following eigenvalue problem

$$L\phi \equiv \epsilon^2 \phi_{yy} + Q\prime(w_H)\phi = \lambda\phi, \tag{35}$$

$$\phi_y(\pm 1) = 0. \tag{36}$$

If we differentiate (17) with respect to y we find $Lw'_H = 0$. So the operator L posed on an unbounded domain has a eigenvalue $\lambda = 0$ with eigenfunction $\phi = w'_H$. Since w_H is a monotonic function connecting the two equilibria, w'_H must be of one sign. Thus it must be the principal eigenvalue. Since w'_H fails to satisfy the boundary conditions of (35) by only exponentially, small terms we expect there to be an exponentially small eigenvalue with eigenfunction ϕ_0 exponentially close to w'_H. We must determine the sign of the perturbed eigenvalue in order to determine the stability of the heteroclinic orbit.

We now construct this eigenfunction using boundary layer correction terms. In the interior of the domain we expect the eigenfunction to be very close to w'_H, the correction terms should be localized to the area near the boundaries. We thus write,

$$\phi_0 \sim C \left(w'_H(\epsilon^{-1}y) + \phi_-(\epsilon^{-1}(y+1)) + \phi_+(\epsilon^{-1}(1-y)) \right). \tag{37}$$

We define boundary layer coordinates $\eta_- = \epsilon^{-1}(y + 1)$ and $\eta_+ = \epsilon^{-1}(1 - y)$.

The boundary layer correction term will then satisfy,

$$\phi''_- - \nu^2_- \phi_- = 0, \quad 0 \le \eta_- < \infty, \tag{38}$$

$$\phi'_-(0) = -w''_H(-1) \sim -a_- \nu^2_- e^{-\frac{\nu_-}{\epsilon}}, \tag{39}$$

$$\phi''_+ - v_+^2 \phi_+ = 0, \quad 0 \le \eta_+ < \infty, \tag{40}$$

$$\phi'_+(0) = w''_H(1) \sim -a_+ v_+^2 e^{-\frac{v_+}{\epsilon}}. \tag{41}$$

The solution to (38) are given by,

$$\phi_\pm(\eta_\pm) \sim a_\pm v_\pm e^{-\frac{v_\pm}{\epsilon}} e^{-v_\pm \eta_\pm}. \tag{42}$$

Now we can start to estimate the small eigenvalue. First we define the dot product as $(f,g) = \int_{-1}^{1} f(y)g(y)\, dy$. We then have the identity

$$(u, Lv) = \epsilon^2 (uv' - u'v)\big|_{-1}^{1} + (Lu, v). \tag{43}$$

We apply this identity to the function w'_H and ϕ_0 to get

$$\lambda_0(w'_H, \phi_0) = -\epsilon w''_H \phi_0 \big|_{-1}^{1} + (Lw'_H, \phi_0). \tag{44}$$

Since $Lw'_h = 0$ and $\phi_0 \sim w'_H$ in the interior of the domain, we have the following asymptotic estimate,

$$\lambda_0 \sim -\frac{\epsilon w''_H \phi_0 \big|_{-1}^{1}}{C(w'_H, w'_H)}. \tag{45}$$

Near $x = \pm 1$, we have that $\phi_0(\pm 1) \sim (w'_H(\pm 1) + \phi_\pm(0)) \sim 2a_\pm v_\pm e^{-v_\pm \epsilon^{-1}}$. Using all our asymptotic estimates we find that,

$$\lambda_0 \sim \frac{2}{\int_{-\infty}^{\infty} w'_H(y)^2 dy} \left(a_+^2 v_+^3 e^{-\epsilon^{-1} 2v_+} + a_-^2 v_-^3 e^{-\epsilon^{-1} 2v_-} \right), \text{ as } \epsilon \to 0. \tag{46}$$

As can be seen from (46), the principle eigenvalue is positive and thus the heteroclinic orbit is unstable. However the eigenvalue is exponentially small and we can thus expect that a heteroclinic solution may persist for long times.

In this section, we have shown that a heteroclinic solution is possible for a single morphogen with self regulation, but the requirements for the existence make such a system unlikely to exist in a natural setting. The restrictions on the auto inhibition function are far too severe to make this a viable alternative. Even if these restrictions are satisfied, the heteroclinic will be unstable and must eventually collapse.

5 Numerical Simulations

In the previous section, we found that a steady-state solution in which the two morphogens are confined to distinct regions in not a practical possibility with just auto-activation. We would like to show that the formation of such solutions is possible when in addition to auto-activation, the two morphogens mutually cross-inhibit each others production. The numerical method is based on the method of lines with a central difference on the diffusion terms and a second-third order adaptive Runge-Kutta time integrator.

There are four pairs of biological parameter values in the model, excluding any for the activation and inhibition, for Wg and BMP respectively. In the numerical simulation, we use the same rate constants and diffusivity for both Wg and BMP. The size of the tissue is x_{max} 0.02 cm ([3]). The diffusion coefficients for Wg and BMP are chosen to be the same: $D_b = 1 \times 10^{-7}$ cm^2 / s based on the measurement [27]; The rate constants are $f_w = 1 \times 10^{-5}$/s, $hw = 0.12/(s\mu M)$, $\gamma_w = 5 \times 10^{-4}$/s, and the total receptor concentration is $R_d = 1\mu M$ [14] [18]. For the initial conditions we set the concentration of bound receptor to be uniformly zero. We set the initial concentration of free morphogen to the following linear gradient:

$$
\begin{aligned}
W(x) &= \frac{\overline{w}(x+0.02) + \widehat{w}(0.02-x)}{0.04}, \\
B(x) &= \frac{\overline{b}(x+0.02) + \widehat{b}(0.02-x)}{0.04},
\end{aligned}
$$

where $\overline{w}, \widehat{w}, \overline{b}$ and $\widehat{b}$ are defined in (12) and (13).

The parameters we will vary are those dealing with activation/inhibition. Figure 4, Figure 5, Figure 7, Figure 9 are graphs of numerical solutions to (1). In each figure we provide 20 concentration profiles equally spaced in time. Initially we set no bound morphogen and a linearly decaying free morphogen concentration profile. The initial condition is displayed in green, the last time step is displayed in red and intermediate steps are displayed in blue.

In this first set of numerical simulations of (1), we demonstrate the robustness of the solution by repeating the simulation with twice the maximum production rates.

The result that we need m, $n \geq 2$ is only proven for a single morphogen with no external inhibition, however numerical results suggest that the requirement m, $n \geq 2$ is also true for the full system. Setting just one of the values to 1 results in an unstable front (see Figure 5).

In Figure 7 and Figure 9, we demonstrate simulations with one cross-inhibition and one auto-activation disabled. In both cases the fronts are unstable and move across the domain until the solution is spatially homogeneous.

In Figure 5, Figure 7 and Figure 9, the system has not reached a steady-state by the end of the run. This is done in order to display the initial transient in which the gradient vanishes. In Figure 6, Figure 8 and Figure 10 we repeated the respective simulations with much larger time-steps to demonstrate the convergence to equilibrium.

Modeling Regeneration

Based on this model, auto-activation is insufficient to maintain mutually exclusive territories of *wg* and *dpp* production. Stable sharp boundaries of wg and dpp expression are dependent on both auto-activation and cross inhibition. We tested whether this GRN could describe the phenotypes produced by genetically modifying *wg* and/or *dpp* production and/or signaling. We will now look at the models ability to capture the behavior of various experimental mutations observed in [6]. These mutations will be mimicked in the model by altering the value of either

or both of Act and Inh on specified subintervals of the domain. In all cases, the experimental results are well represented by the appropriately modified version of (1). Each graph represents 20 equally spaced time steps. The initial condition is given in green. The final state is given in red. All intermediate states are displayed in blue. Where available, the results of the mutation are also displayed.

A mitotic clone of dsh blocks Wg signal transduction. In the model, this can be mimicked by absence of the WG receptor in a small region. In the region $0.013 < x < 0.018$ we set wr and wrt to 0 (Figure 11). This can also be modeled by defining WR as inactive or unable to signal (Figure 12). In the second simulation, the wg receptors in a part of the ventral region can bind with wg, but there is no response. The mutation is in the region $0.01 < x < 0.014$ (Figure 12). When this occurs in a clone of cells in the fly leg, it results in pattern duplications that are predicted by the GRN modeled here. Similarly, the model predicts that production of WG at high levels in the dorsal dpp/bmp domain also produces pattern duplications. For this simulation (Figure 13), Wg production is fixed at a high rate independent of receptor binding for the region $0.012 < x < 0.016$. The model predicts patterning duplications that mimic those seen in fly legs where a clone of dorsal cells is mutant for an antagonist of Wg signaling (GSK/sgg). In these cells, Wg signaling is ectopically activated.

6 Discussions

As we have seen from the analysis, although it is possible for a single morphogen to form a territory solution based only on auto-regulation, such a situation is unstable and unlikely. However, numerical simulations of two interacting morphogens show that morphogen territory solutions are not only possible, but very robust. The only requirement is that the interaction must be strong. If we use a Hill equation to model the interaction, we require a Hill coefficient of at least two. Such a coefficient would be achieved by requiring two or more morphogen molecules bound to a receptor for activation/inhibition to be turned on.

The study of the full system is still open. Since the diffusion coefficients of the two morphogens are of the same order, it is not possible to separate (7) into two second order equations. It may be possible to force symmetries into the system with an appropriate parameter choices, however there is no numerical evidence that such restrictions are required.

Acknowledgment

References

1. Brook WJ, Cohen SM. Antagonistic interactions between wingless and decapentaplegic responsible for dorsal-ventral pattern in the drosophila leg. Science 1996;273(5280):1373–1377. [PubMed: 8703069]

2. Diaz-Benjumea FJ, Cohen SM. Wingless acts through the shaggy/zeste-white 3 kinase to direct dorsal-ventral axis formation in the drosophila leg. Development 1994;120(6):1661–1670. [PubMed: 8050372]

3. Entchev EV, Schwabedissen A, Gonzalex-Gaitan M. Gradient formation of the tgf-beta homolog dpp. Cell 2000;103:981–991. [PubMed: 11136982]

4. Gierer A, Meinhardt H. A theory of biological pattern formation. Kybernetik 1972;12:30–39. [PubMed: 4663624]

5. H M. Space-dependent cell determination under the control of morphogen gradient. J Theor Biol 1978;74(2):307–321. [PubMed: 713579]

6. Heslip TR, Theisen H, Walker H, Marsh J. Shaggy and dishevelled exert opposite effects on wingless and decapentaplegic expression and on positional identity in imaginal discs. Development 1997;124 (5):1069–1078. [PubMed: 9056781]

7. Hill AV. The combinations of haemoglobin with oxygen and with cobon monoxide. I. J. Physiol 40:iv–vii.

8. Immergluck K, Lawrence PA, Bienz M. Induction across germ layers in drosophila mediated by a genetic cascade. Cell 1990;62(2):261–268. [PubMed: 1973634]

9. Jiang J, Struhl G. Complementary and mutually exclusive activities of decapentaplegic and wingless organize axial patterning during drosophila leg development. Cell 1996;86(3):401–409. [PubMed: 8756722]

10. Johnston LA, Schubiger G. Ectopic expression of wingless in imaginal discs interferes with decapentaplegic expression and alters cell determination. Development 1996;122(11):3519–3529. [PubMed: 8951067]

11. Klingensmith J, Nusse R, Perrimon N. The drosophila segment polarity gene dishevelled encodes a novel protein required for response to the wingless signal. Genes Dev 1994;8(1):118–130. [PubMed: 8288125]

12. Koch AJ, Meinhardt H. Biological pattern formation: from basic mechanisms to complex structures. Reviews of Modern Physics 1994;66(4):1481–1507.

13. Lander AD, Nie Q, Vargas B, Wan FYM. Aggregation of a distributed source in morphogen gradient formation. Studies in Applied Mathematics 2005;114(4):343–374. [PubMed: 17372620]

14. Lander AD, Nie Q, Wan F. Do morphogen gradients arise by diffusion? Developmental Cell 2002;2 (6):785–796. [PubMed: 12062090]

15. Lander AD, Nie Q, Wan FYM. Spatially distributed morphogen production and morphogen gradient formation. Math. Biosci. Eng 2005;2(2):239–262.

16. Lou Y, Nie Q, Wan FM. Effects of sog on dpp-receptor binding. SIAM J. on Applied Math 2005;66 (5):1748–1771.

17. Meinhardt, H. Models of biological pattern formation. London; New York: Academic Press; 1982.

18. Mizutani C, Nie Q, Wan F, Zhang Y, Vilmos P, Bier E, Marsh L, Lander A. Origin of the BMP activity gradient in the *drosophila* embyro. Development Cell 2005;8(6):915–924.

19. Morimura S, Maves L, Chen Y, Hoffmann FM. Decapentaplegic overexpression affects drosophila wing and leg imaginal disc development and wingless expression. Dev Biol 1996;177(1):136–151. [PubMed: 8660883]

20. Penton A, Hoffmann FM. Decapentaplegic restricts the domain of wingless during drosophila limb patterning. Nature 1996;382(6587):162–164. [PubMed: 8700205]

21. Struhl G, Basler K. Organizing activity of wingless protein in drosophila. Cell 1993;72(4):527–540. [PubMed: 8440019]

22. Syed A, Theisen H, Nguyen B, Lukasovich T, Purcell J, Srivastava G, Irons D, Gaudenz K, Nie Q, Wan F, Waterman M, Marsh JL. Pattern of dpp morphogen expression maintained by armadillo/tcd mediated repression in response to wg signaling. PLoS One 2007;2(1):e142. [PubMed: 17206277]

23. Theisen H, Haerry TE, O'Connor M, Marsh JL. Developmental territories created by mutual antagonism between wingless and decapentaplegic. Development 1996;122(12):3939–3948. [PubMed: 9012514]

24. Theisen H, Purcell J, Bennett M, Kansagara D, Syed A, Marsh J. Dishevelled is required during wingless signaling to establish both cell polarity and cell identity. Development 1994;120(2):347–360. [PubMed: 8149913]

25. Turing A. The chemical basis of morphogenesis. Phil. Trans. Roy. Soc. B 1952;32:37–72.

26. Umulis DM, Serpe M, O'Connor MB, Othmer HG. Robust, bistable patterning of the dorsal surface of the Drosophla embyo. Developmental Biology 2006;103(31):11613–11618.

27. Wang Z, Marcu O, Berns MW, Marsh JL. In vivo FCS measurements of lignad diffusion in intact tissues. Proc. SPIE 2004;5323:177–183.

28. Webb SD, Owen MR. Oscillations and patterns in spatially discrete models for developmental intercellular signalling. J. Math. Biol 2004;48:444–476. [PubMed: 15052506]

29. Weiss JN. The Hill equation revisited: uses and misues. FASEB Journal 1997;11:835–841. [PubMed: 9285481]

30. Wilder EL, Perrimon N. Dual functions of wingless in the drosophila leg imaginal disc. Development 1995;121(2):477–488. [PubMed: 7768188]
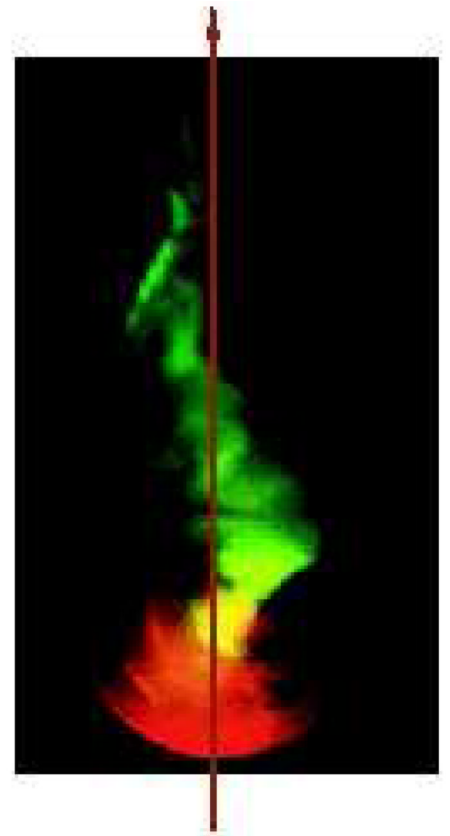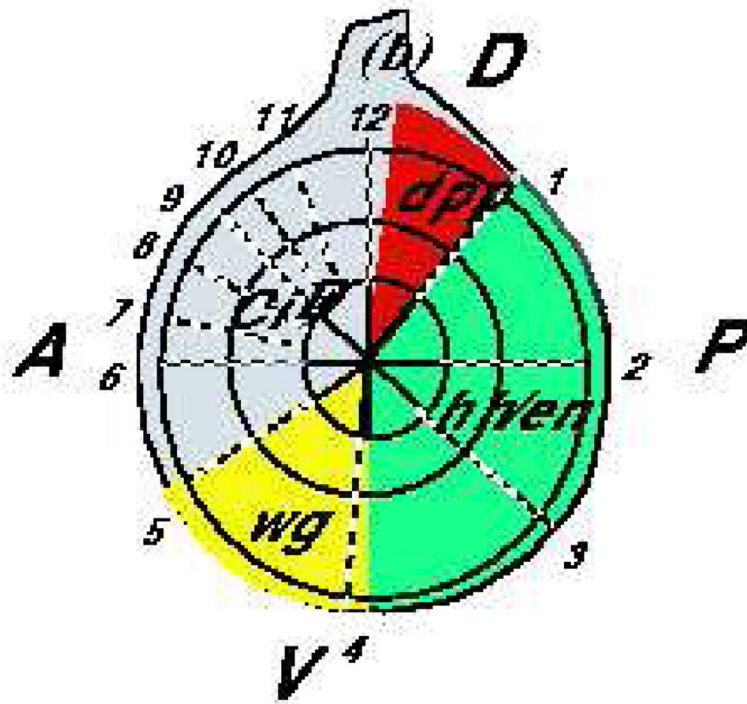
(a)

(b)

Fig. 1.
(a–b) leg imaginal discs with anterior to the left and dorsal up. (a) schematic picture of a leg imaginal disc; (b) production of both bmp/dpp (green) and wg (red). The line indicates the x-axis of the proposed model.
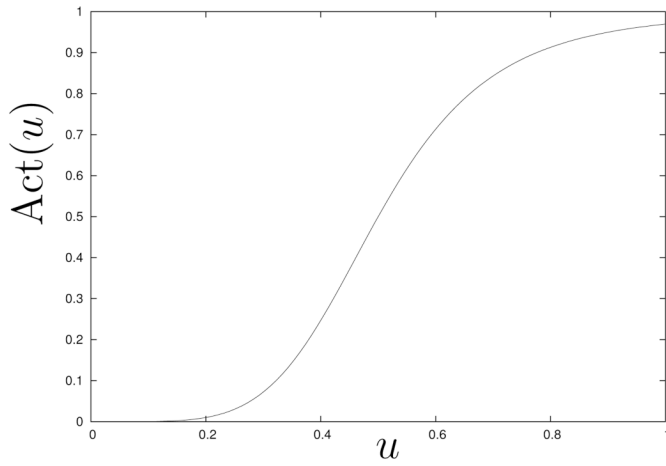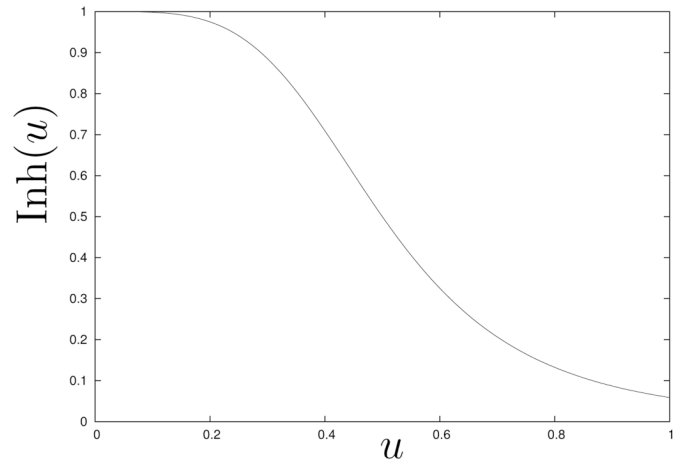
2.1: $\mathrm{Act}(u)$ 2.2: $\mathrm{Inh}(u)$

Fig. 2.

Sample graphs of the functions Act and Inh with $m = 4$, $u_0 = \dfrac{1}{2}$, $K_{max} = 1$ and $K_{min} = 0$.
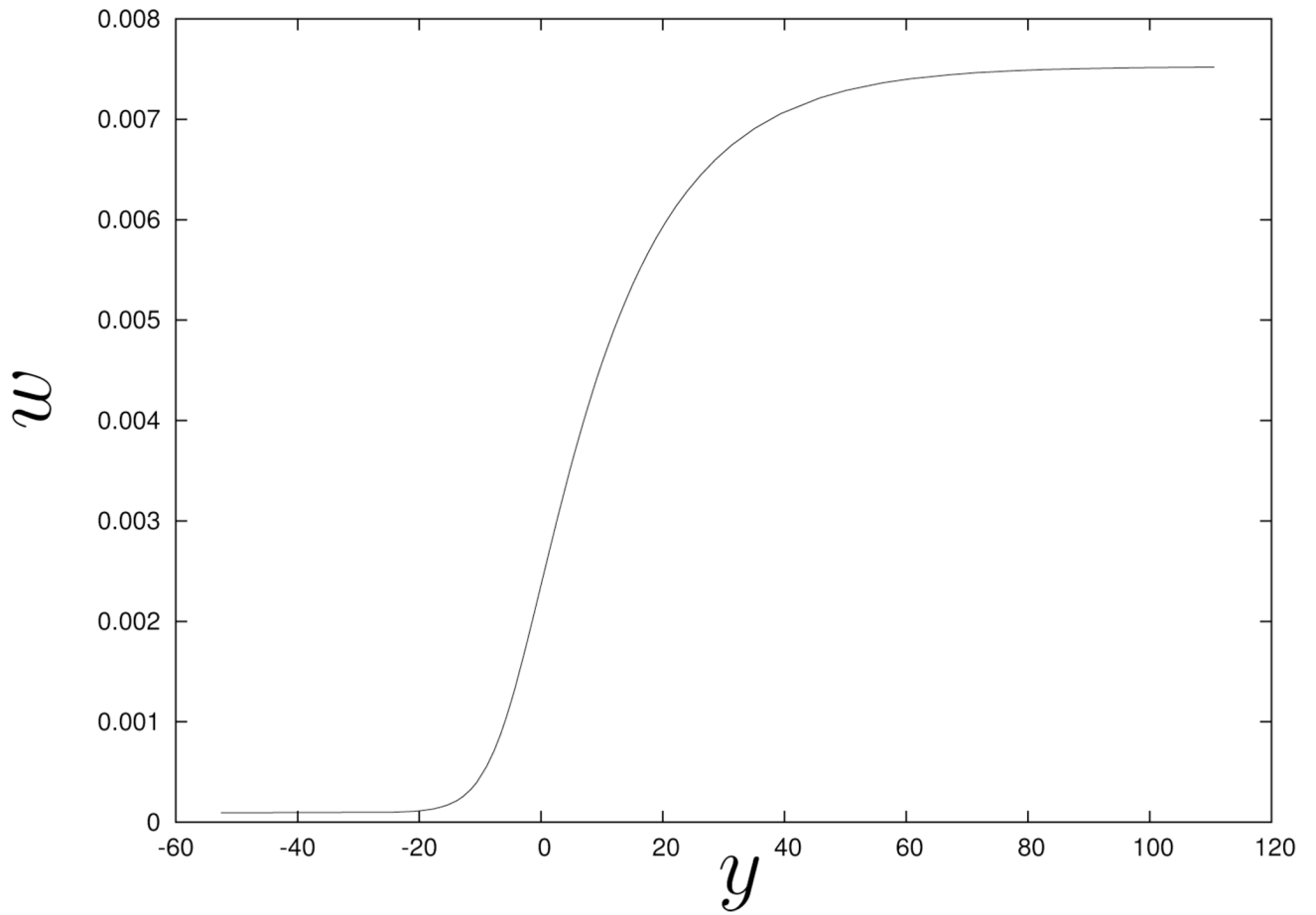
Fig. 3.
Approximation of the heteroclinic connection for (17). For this simulation, $I = 0.0099805992$, $m = 2$, $K_{max} = 0.051$, $K_{min} = 0.001$. For these values, $w_- \sim= 0.0000950097$ and $w_+ \sim 0.0075233436$.
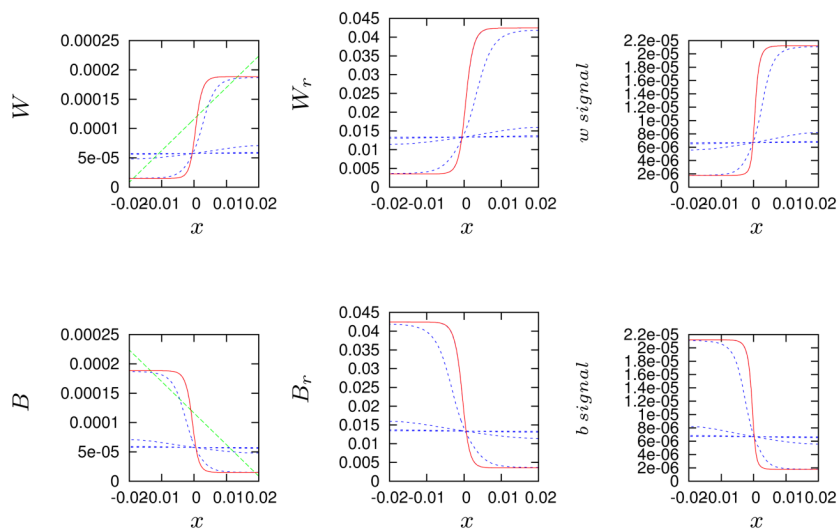
4.1: $k_{max} = 0.005$
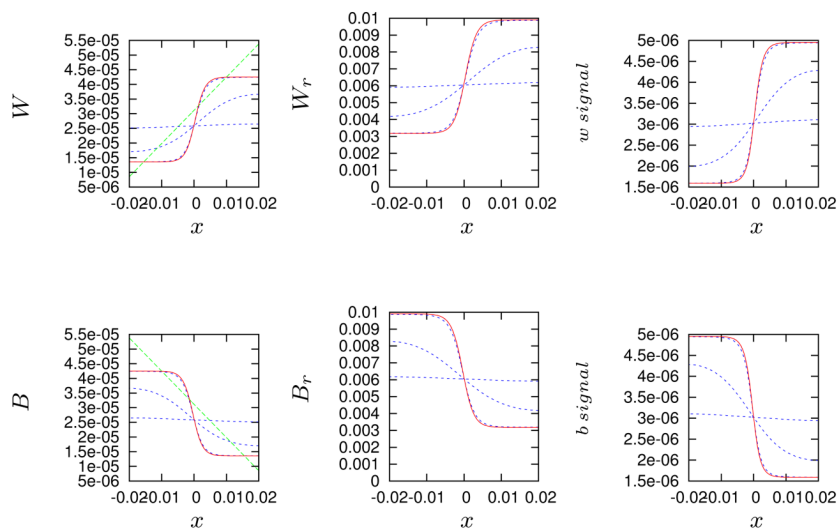
4.2: $k_{max} = 0.0025$

Fig. 4.
Numerical simulation of full system with parameter values $K_{min} = 0.0001$ $m = n = 3$. In both runs the final time is $t = 150000$ seconds. The plots of w signal and b signal are plots of the production rates of w and b respectively.
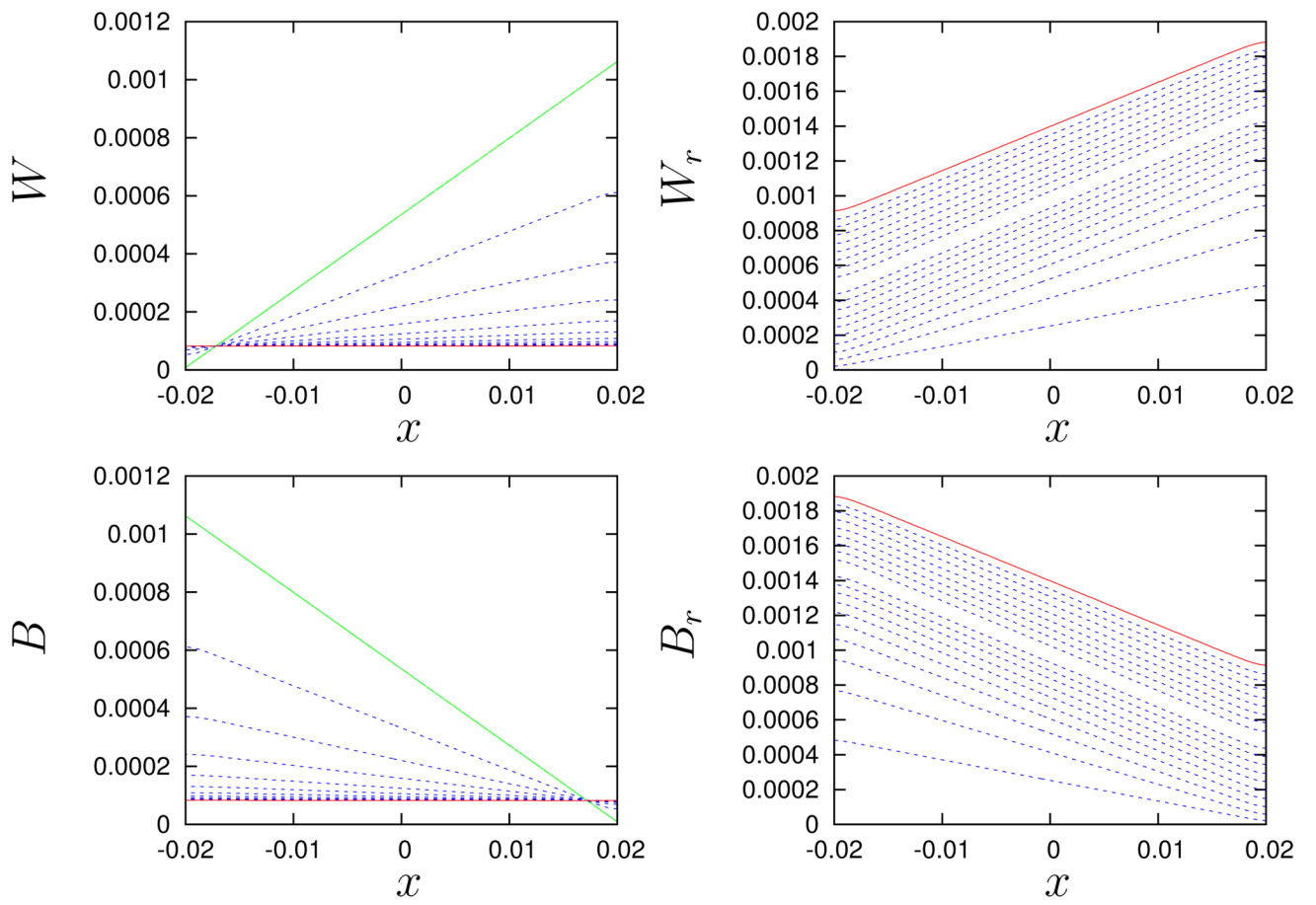
Fig. 5.
A numerical simulation of system (1) with $m = 1$, $n = 3$, $K_{min} = 0.001$ and $K_{max} = 0.01$. The final time step is at $t = 100$ seconds.
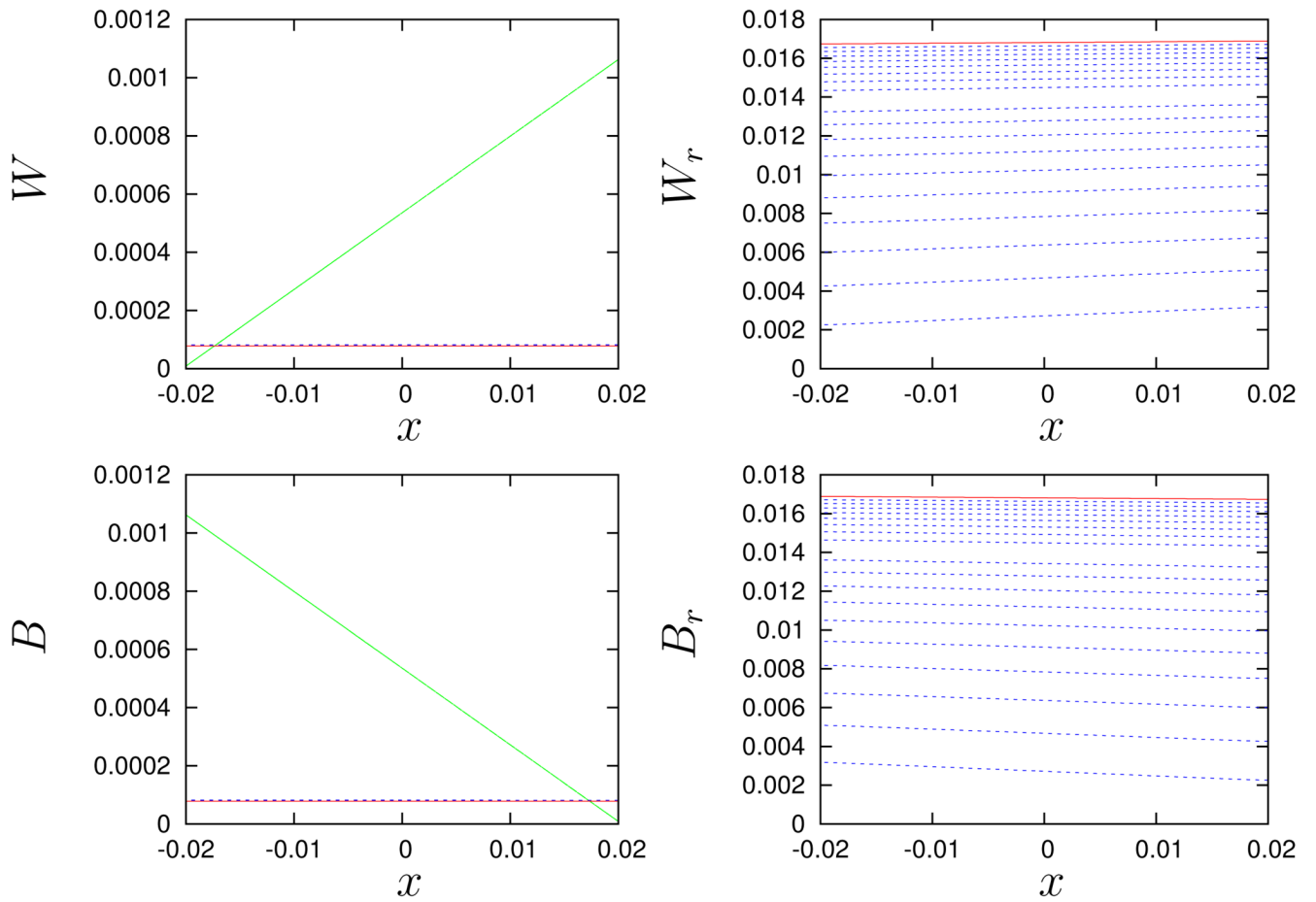
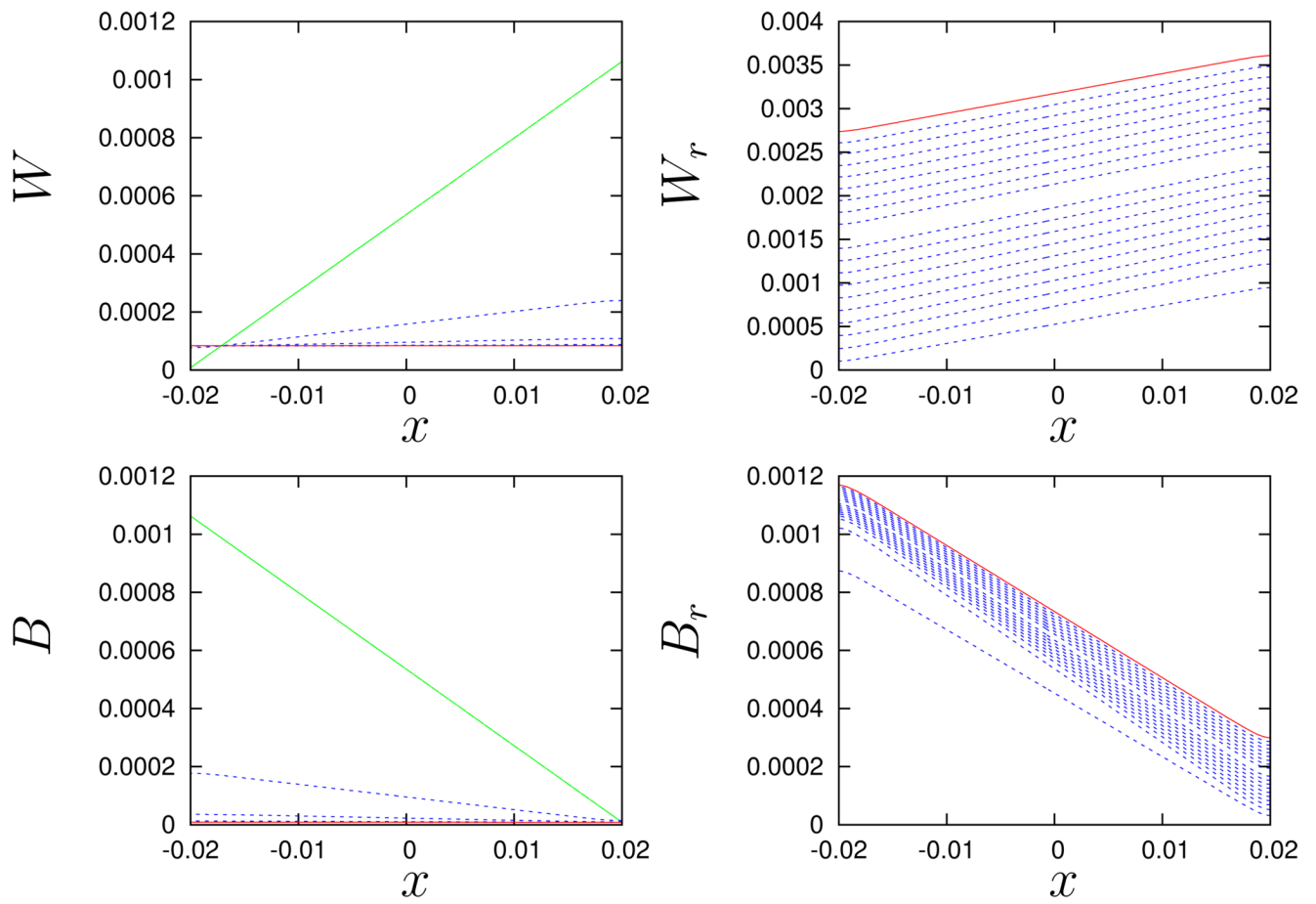**Fig. 6.**
A continuation of the simulation given in Figure 5 with a much larger time-step in order to display the convergence to an equilibrium. The final time step is at $t = 5000$ seconds.
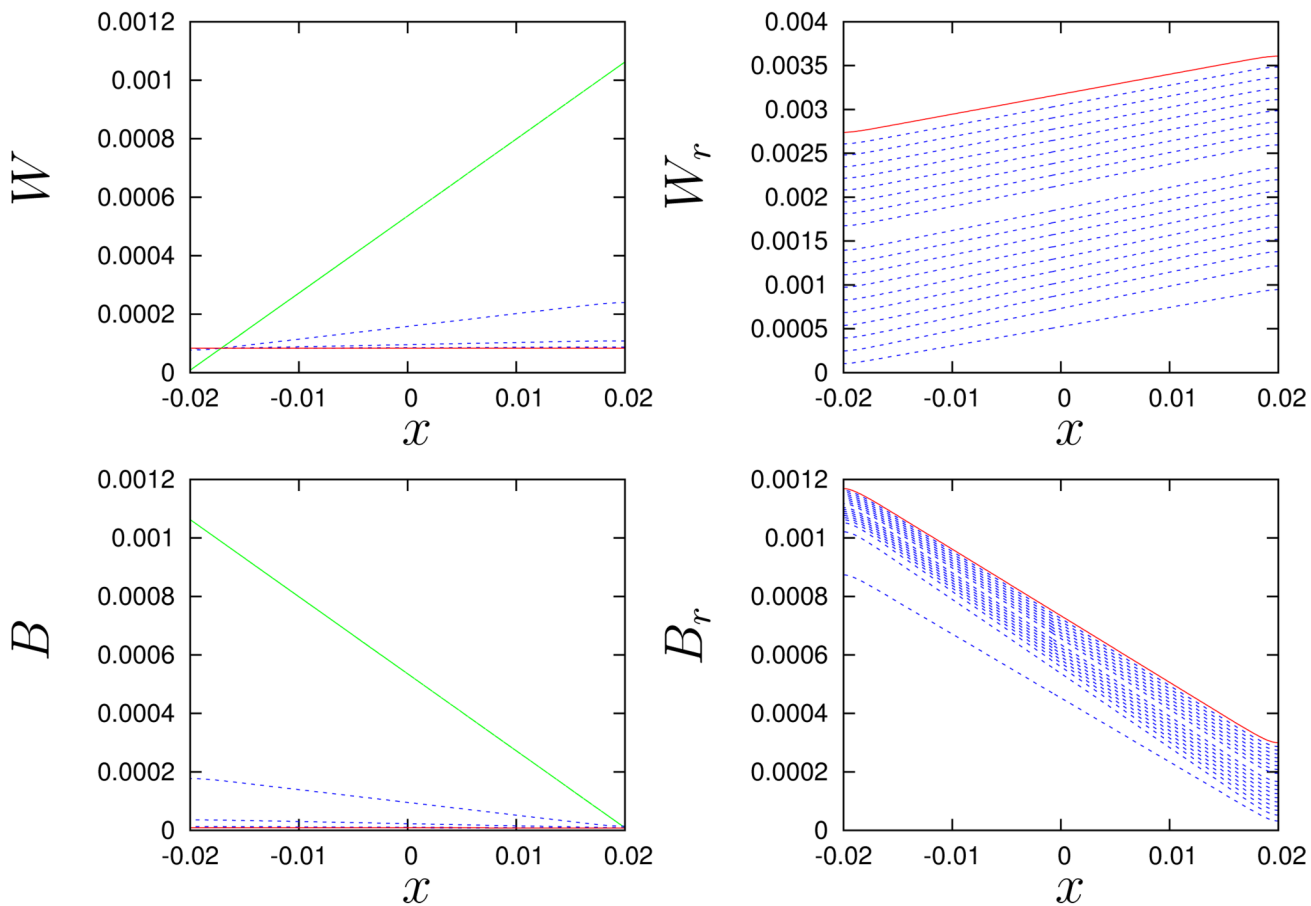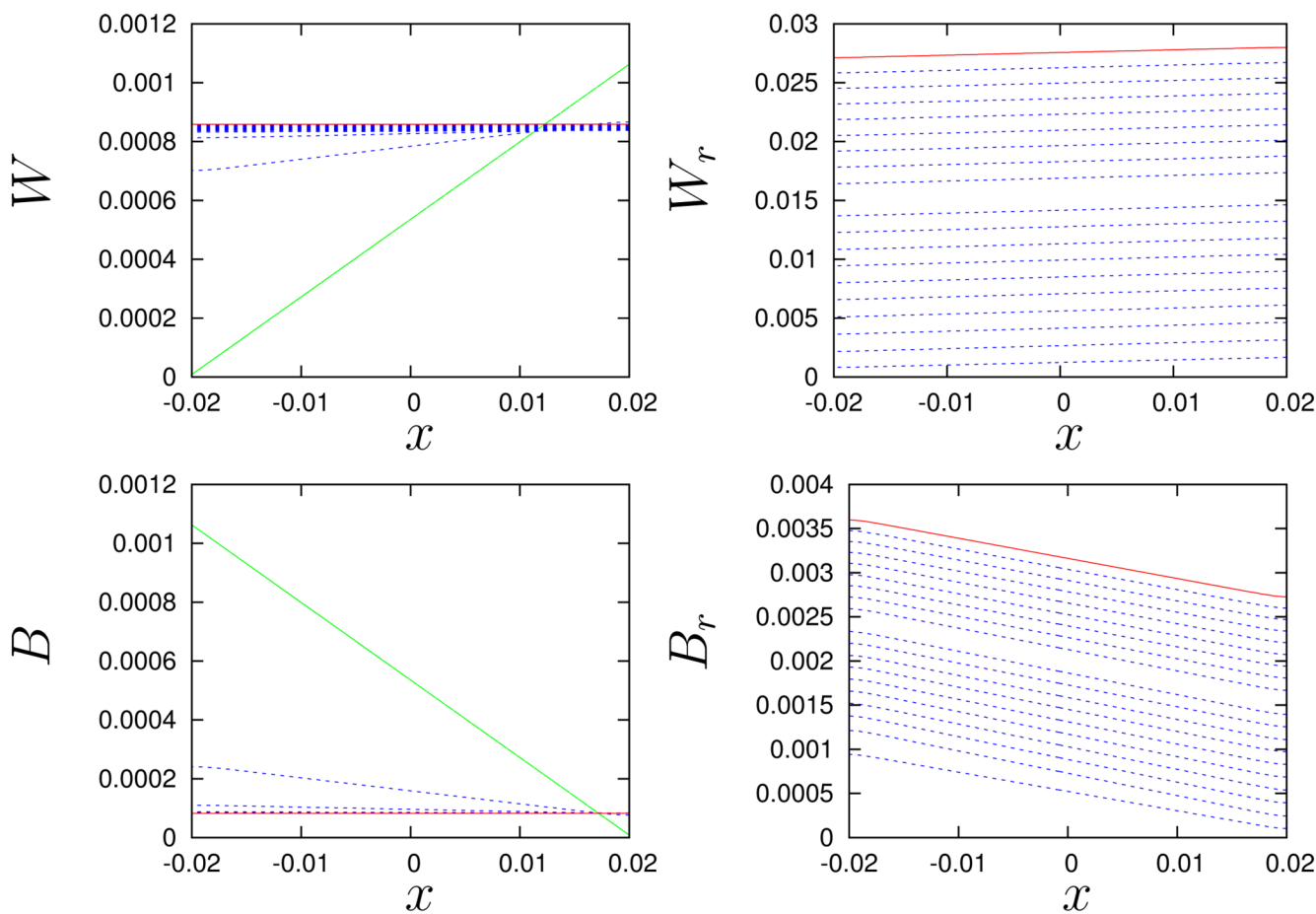
Fig. 7.
A numerical simulation of system (1) for $m = 3$, $n = 3$ and cross-inhibition of B_r on W shut off. The values of K_{max} and K_{min} are adjusted to produce maximum and minimum production rates of 0.01^2 and 0.001^2 respectively for all terms. Final time step is at $t = 300$ seconds.
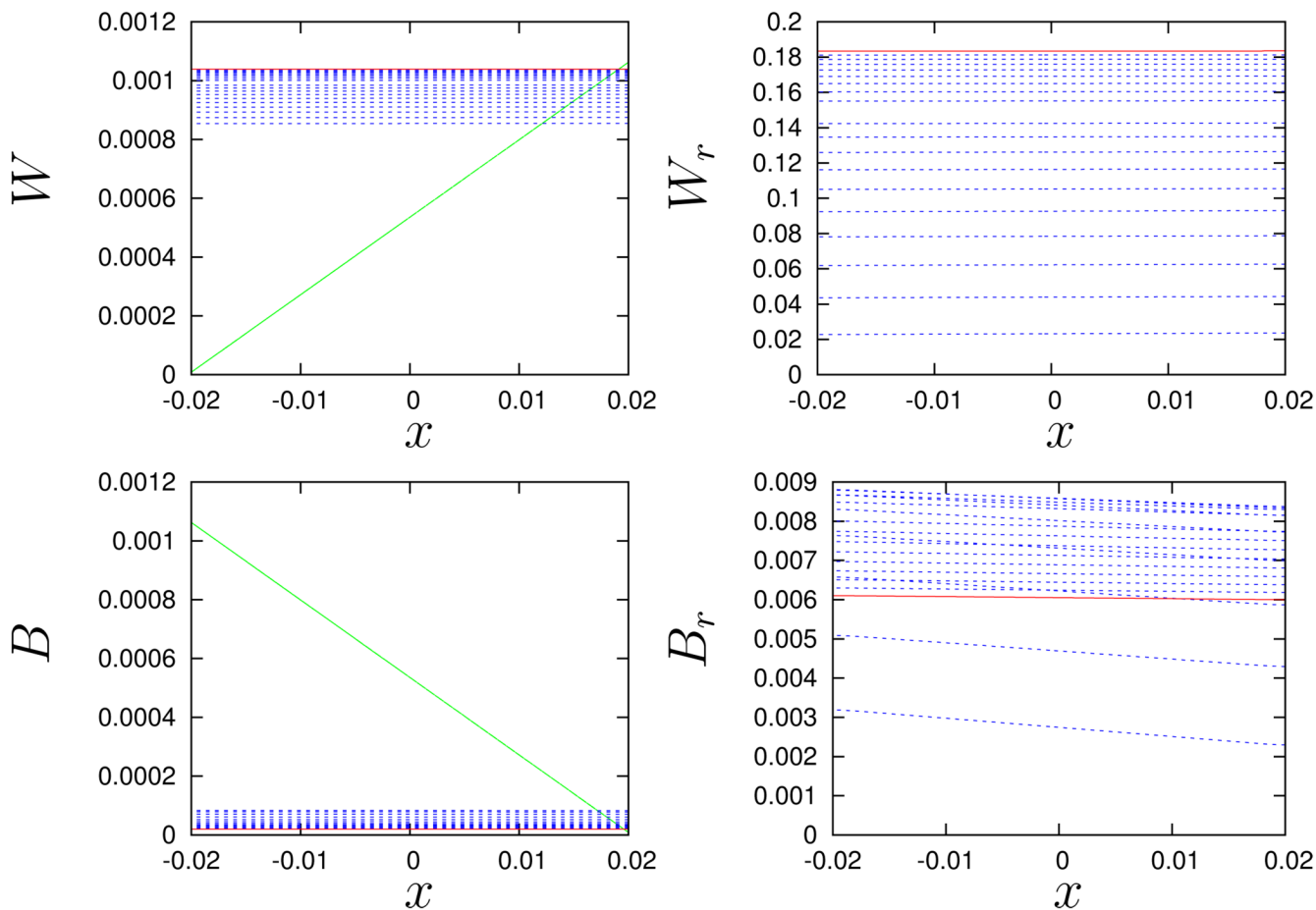
Fig. 8.
A continuation of the simulation given in Figure 7 with a much larger time-step in order to display the convergence to an equilibrium. Final time step is at $t = 5000$ seconds.

Fig. 9.
A numerical simulation of system (1) for $m = 3$, $n = 3$ and auto-activation of W shut off. The values of K_{max} and K_{min} are adjusted to produce maximum and minimum production rates of 0.01^2 and 0.001^2 respectively for all terms. Final time step is at $t = 300$ seconds.

Fig. 10.
A continuation of the simulation given in Figure 9 with a much larger time-step in order to display the convergence to an equilibrium. Final time step is at $t = 5000$ seconds.
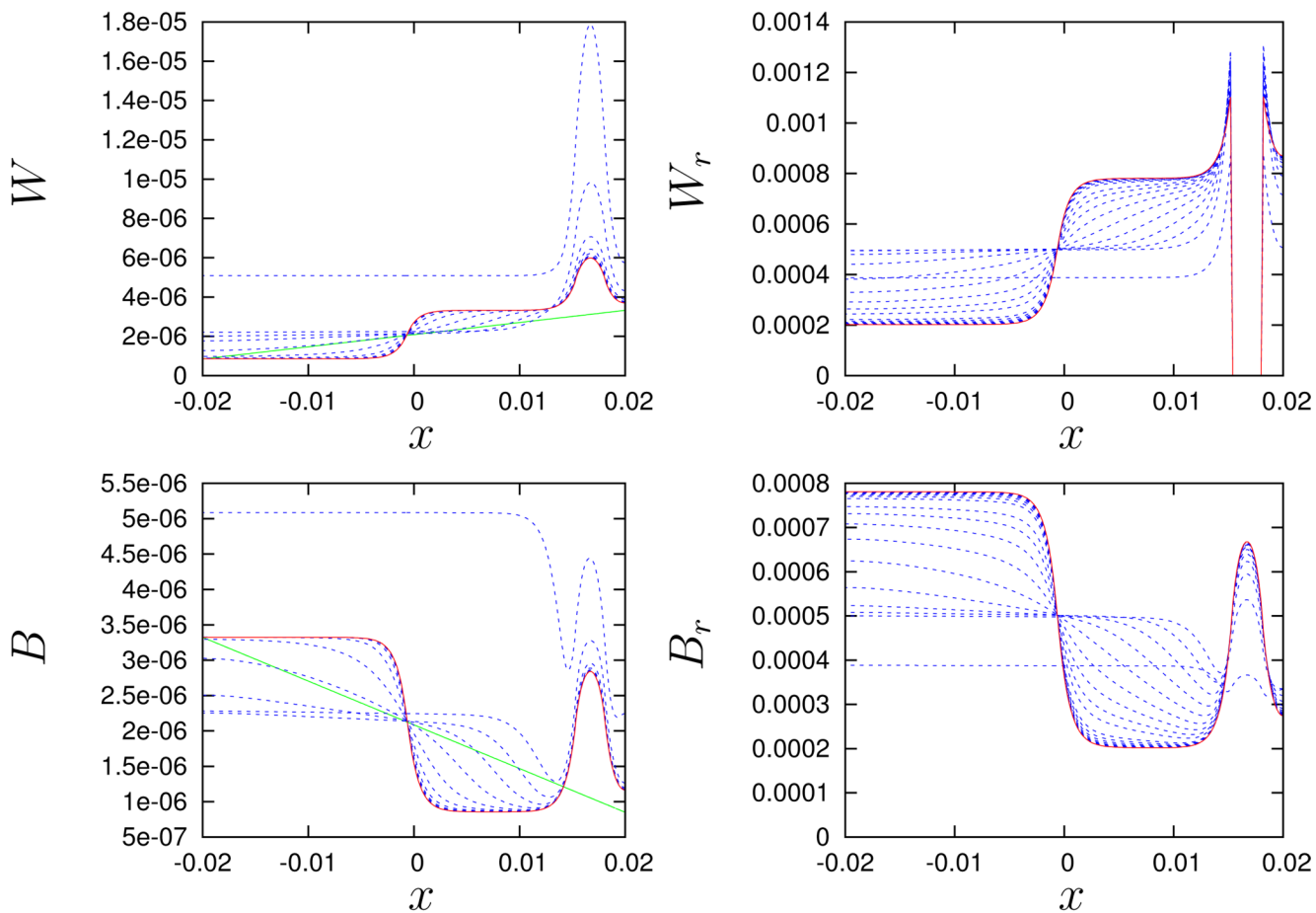
Fig. 11.
In this simulation there are no Wg receptors for $0.012 < x < 0.016$. The final time step is at $t = 15000$ seconds. The slight localized increase in W is due to lack of receptor to bind with. The localized increase in B is due to the local lack of inhibition.
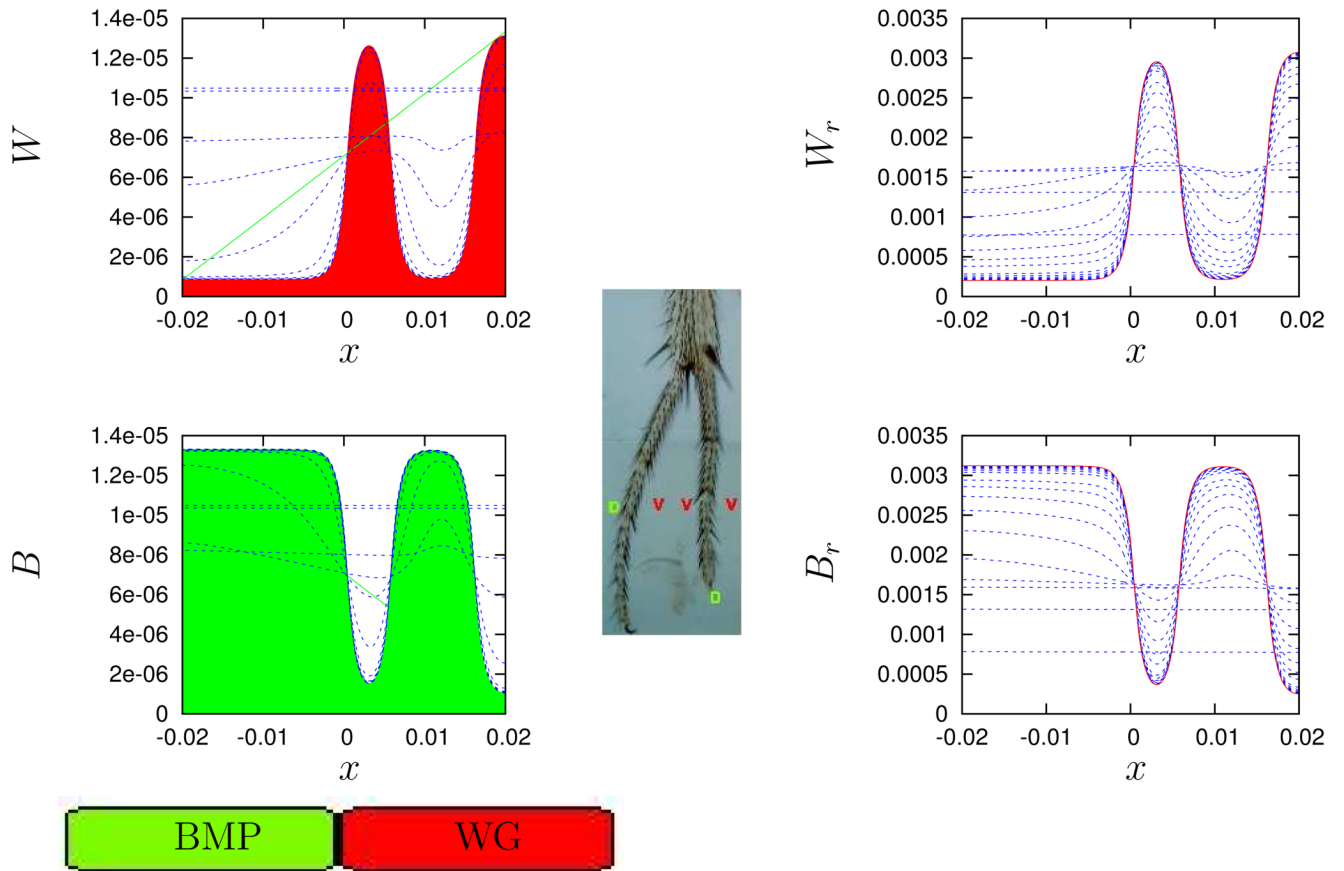
Fig. 12.
Simulation of region with defective Wg receptors in the region $0.013 < x < 0.018$. Since Wg is still able to bind to its receptor there is no localized increase as seen in Figure 11. The final time step is at $t = 15000$ seconds. The experimental image is from [6].
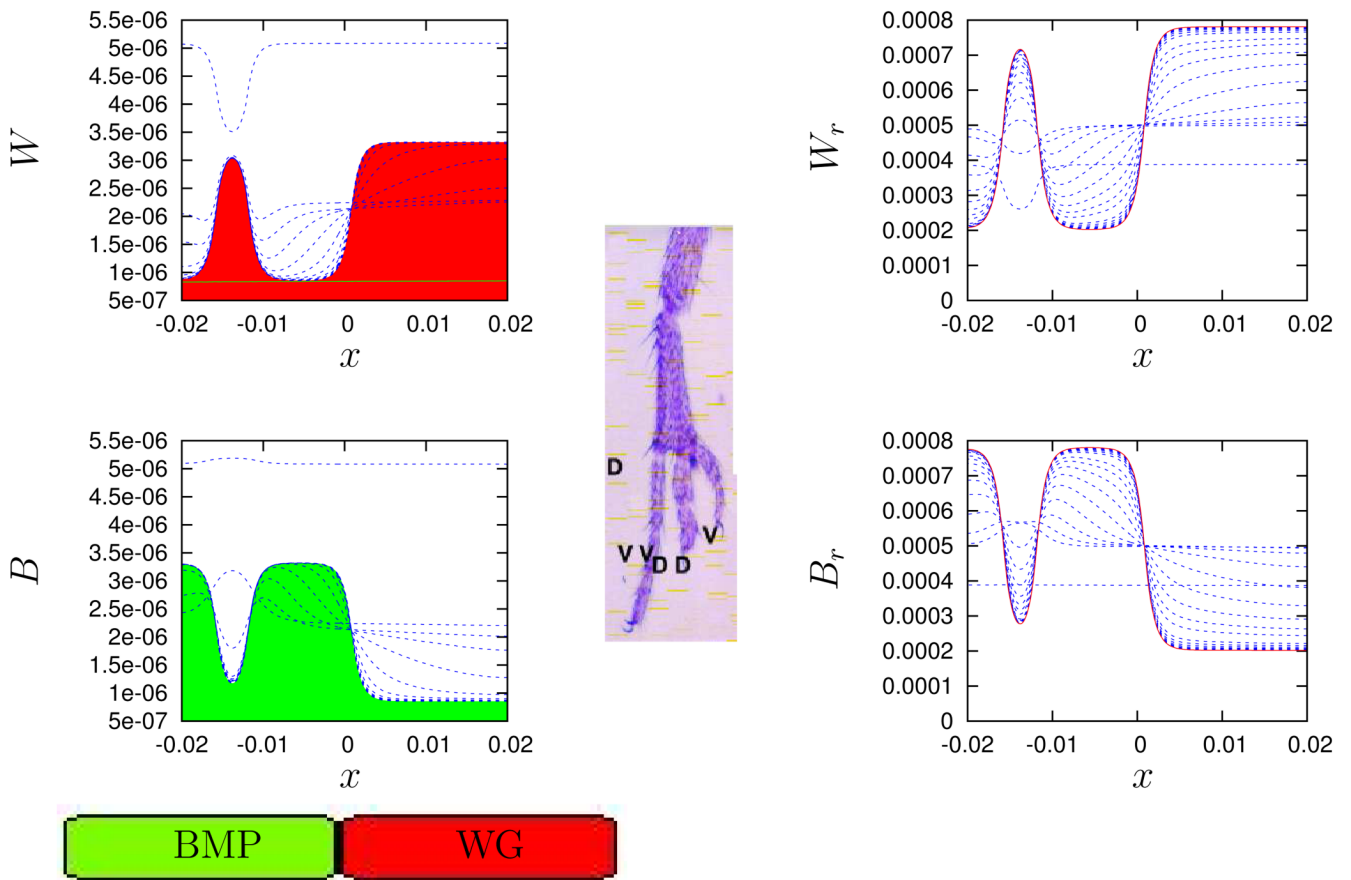
Fig. 13.
Simulation of region with Wg production set to its maximum rate independent of receptor binding for $0.012 < x < 0.016$ causing localized increases in W and decreases in B. The final time step is at $t = 15000$ seconds. The experimental image from [6].

Table 1

Abbreviations Used

W	The concentration of free Wg.
W_r	The concentration of bound Wg.
B	The concentration of free BMP.
B_r	The concentration of bound BMP.
R_W	The total number of Wg receptors.
R_B	The total number of BMP receptors.
D_W	The diffusivity of Wg.
D_B	The diffusivity of BMP.